Indian Journal of Pure & Applied Physics
Vol. 61, August 2023, pp. 659-670
DOI: 10.56042/ijpap.v61i8.952

Synthesis and Characterization of Fe_3O_4-oleate/Poly (vinyl alcohol) Nanocomposites for Electrical Applications

Kanakaraj T M[a,b], Rajashekhar F Bhajantri[a]*, Chetan Chavan[c], Soumya Bulla[d], Mallikarjun Anandalli[e], Malatesh S Pujar[a] & Mangesh S Jadhav[b]

[a]Department of Physics, Karnatak University Dharwad 580 003, Karnataka, India

[b]Department of Physics, J S S Arts, Science and Commerce College, Gokak 591 307, Karnataka, India

[c]Department of Physics, V.V. Sangha's Kottureshwara Degree College, Kottur 583 134, Karnataka, India

[d]Department of Physics, Davangere University, Shivagangotri, Davangere 577 007, Karnataka, India

[e]Inter University Centre for Nanoscience and Nanotechnology (IIUCNN), Mahatma Gandhi University, Kottayam 686 560, Kerala, India

Received 15 May 2023; accepted 3 July 2023

Herein we report the Fe_3O_4-oleate (Fe-OA) nanoparticles (NPs) incorporated poly (vinyl alcohol) (PVA), a series of highly flexible nanocomposites (Fe-OA-PVA) were prepared by the solution casting technique. The nanocomposites were fabricated with different weights per cent (0.25 wt. %, 0.5wt. %, and 0.75wt. %, 1wt. %, and 2wt. %, respectively) of Fe_3O_4-OA into the PVA matrix. The synthesized nanocomposites were characterized using FTIR, UV–Vis, XRD, Contact angle, Impedance spectroscopy, SEM and EDS. UV-Vis spectra initially confirmed the interaction of Fe-OA NPs into the PVA matrix by observing peaks at 223nm, 325nm and 410nm. The FTIR investigation uncovered evidence of an interaction between the NPs and the PVA polymer matrix. The incorporation of NPs into a polymer matrix shows an enhancement in various properties due to its nature. The surface properties of the composites were studied using the contact angle technique. The electric properties of Fe_3O_4-oleate/PVA nanocomposite films were estimated using impedance spectroscopy. Due to the dispersion of Fe_3O_4-oleate NPs into the PVA matrix, we obtained the polarization in dipoles, resulting in good AC-Conductivity properties. These synthesized nanocomposites may potentially use for electronic applications.

Keywords: Poly(vinyl alcohol); Nanocomposites; Dielectric constant; Electrical property; Fe_3O_4-oleate NPs

1 Introduction

Nanocomposites have become an important research field for the last few decades due to their potential use in producing cutting-edge materials[1,2]. Metal oxide nanoparticles have gained considerable interest because of their unique physicochemical properties. Several metal oxide nanoparticles have been used as filler materials in various polymeric systems to produce significantly different physicochemical properties than the unaltered polymer. These nanoparticles have enhanced properties over bulk materials and can be easily controllable for magnetic field application.[1] Magnetic iron (Fe) NPs offer enormous promise for therapeutic uses such as medication delivery, hyperthermia therapies, and MRI contrast agents for imaging purposes[3]. The metal nanocomposites exhibit induced quantum size effects and can be exploited for enormous applications such as catalysis, electronics, sensors and optoelectronics. Due to potential application in various fields polymer and semiconductor materials have attracted considerable interest as a class of new material. The low-cost and more effectively applicable synthesis of polymer-based nanomaterials is a challenging task in the present scenario.

The biomedical industry has extensively used PVA for various purposes, including cataract lenses, wound care products, artificial cardiac surgery, and operative sutures[3,4]. Such nanomaterials have attracted considerable interest in enormous applications[3,5]. PVA has shown, to this point, characteristics such as non-toxicity, substantial oxygen permeability, biodegradability and beneficial interactions with metal oxide nanoparticles[6]. Eventually, PVA has inadequate mechanical endurance to counteract this disadvantage; it should be chemically cross-linked or incorporated with hydrophilic materials to optimize its mechanical stability. Oleic acid is a water-soluble

*Corresponding authors:
(E-mail: rfbhajantri@gmail.com; rfbhajantri@kud.ac.in)

linear polysaccharide that acts as a cross-linker between Iron Oleate (Fe_3O_4) and PVA[1,3]. Nanoparticle reinforcement in the matrix of polymers enhances mechanical strength and dimensional and thermal resilience. The mechanical, electrical, magnetic, and optical characteristics of reported Fe_3O_4/chitosan/ PVA fibres were investigated[7–9]. Due to its magnetic behaviour – ferromagnetic iron oxide nanomaterials show efficient potential in capacitor applications.

In recent years, new polymer nanocomposite materials with electrical and optical properties have gained more importance[10,11]. These polymer nanocomposites have shown enormous applications due to their unique architecture, exceptional stability, flexibility and ease of preparation[12]. In conventional polymer nanocomposites, the virgin polymers are encapsulated with different weights per cent (wt.%). Nanoparticles were prepared, showing enhanced applications as electrochemical solar cells, electrical conductivity and optical properties[4,13]. PVA is a synthetic polymer which is biodegradable, biocompatible, non-toxic and exhibits swelling in water. These natures decrease thermal stability and also result in decreased electrical and optical properties. Such drawbacks would be overcome by cross-linking with various organic compounds for attaining hydrophobicity and other desired applications[14]. Adding oleic acid, an unsaturated omega-9 fatty acid, to Fe-nanoparticles in a PVA polymer matrix, increased resistance to the disintegration of the polymer in water[1–3]. Also, the high temperature for the flow of electrolytes within a polymer matrix sometimes causes fire and is overruled by the concurrent addition of oleic acid[15].

In the present work, the fabrication of Fe_3O_4 was modified with oleic acid, and then they were incorporated into the PVA matrix at different wt.% by solvent casting method[10,16–18]. These newly fabricated composites were analyzed by various Physico-chemical techniques *viz,* Ultraviolet-Visible (UV-Vis) Spectroscopy, Fourier Transform Infrared Spectroscopy (FTIR), X-ray Diffraction (XRD), Scanning electron Microscopy (SEM) and Energy Dispersive Spectroscopy (EDS) studies to determine their optical, functional, structural, morphological, and elemental analysis respectively. Impedance analysis of synthesized nanocomposites was investigated and resulted in enhancement in the electrical property. In polymer semiconductor research, designed and synthesized novel core-shell nanomaterials with polymer possess high mobility[5,19,20]. Iron oxide nanoparticles exhibit ferromagnetic properties at ambient temperature and exhibit an elevated dielectric constant with minimal dielectric loss, rendering them suitable for use in capacitor applications. Hence, synthesized nanomaterials have shown efficient electric properties which can be used for various applications.

2 Materials and Methods

PVA with molecular weight ~ 125,000g/mol (86-89% hydrolyzed)was procured from Merck Ltd., Mumbai, India. The oleic acid ($C_{18}H_{34}O_2$) ($M_w = 282\ g/mol$) was purchased from Sigma Aldrich Co, India. $FeCl_3$ ($M_w = 162\ g/mol$), Potassium Oleate ($M_w = 320\ g/mol$), Oleyl alcohol($M_w = 268\ g/mol$), Diphenyl ether ($M_w = 170\ g/mol$), acetone($M_w = 58\ g/mol$), n-hexane ($M_w = 86\ g/mol$), chloroform ($M_w = 119\ g/mol$)was obtained from Sigma Aldrich Co, India. The chemicals utilized were of analytical grade and were employed without undergoing additional purification procedures. Deionized water was employed throughout the production of the nanomaterials. Nanoparticles were synthesized using the chemical reduction method[9,18–22]. The chemical structure of PVA and Oleic acid is shown in Fig. 1.

3 Synthesis of Nanomaterials and Their Composites

3.1 Preparation of Iron Oleate Complex

The iron oleate complex was prepared by stirring 1 mmol of ferric chloride and 3 mmol of potassium oleate mixture in a ratio of 2:4:1 (hexane, water, ethanol) for two hours. Further, the mixture was allowed to heat to 80 °C for a period of 30 minutes. Once the mixture has been cooled down at ambient temperature, phase separation occurs, the hexane phase containing the top organic layer of iron oil complex has been removed and washed three times using doubly distilled water in a separating funnel to remove untreated materials. Treatment was done to remove tiny quantities of solvent molecules such as

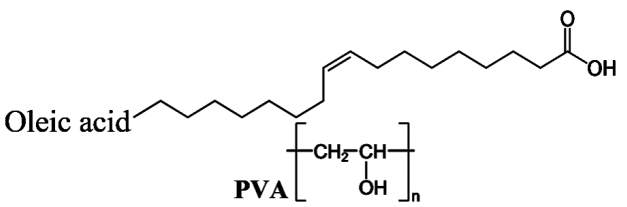

Fig. 1 — Chemical structure of Oleic acid and PVA.

hexane, water and ethanol; the resulting mixture was then dried for 24 hours at 45 °C in a hot air oven. About ~70% of the iron oleate complex in the solution appeared to be pure.

3.2 Iron Oxide (Fe_2O_3) Nanoparticle Synthesis

The chemical reduction was used for the production of Fe_3O_4 nanoparticles initially. As ligands, 2 mmol of iron-oleate complex (1.8 g) was precisely weighed, 2 mmol of oleic acid (0.57 g) was utilized, and 6 mmol of Oleyl alcohol (1.61 g) was disintegrated in diphenyl ether. Using a muffle furnace and a steady heating rate of 10 °C/min, the mixture was elevated to 250 °C for 30 minutes. As a result of the chemical effect, the initial solution changed from light brown to black, proving the formation of nanoparticles of iron oxide with a neutral PH. The nanoparticles were precipitated by adding 50 mL of acetone after the medium containing nanoparticles had cooled rapidly to room temperature (25 °C). The resultant particulates were distinguished by centrifugation and then disseminated in nonpolar solvents such as n-hexane (C_6H_{16}) or chloroform ($CHCl_3$). During the process, Fe_3^+ ions were released from the interior of Fe_3O_4 to its surface. At room temperature, 2 mmol of iron-oleate complex (1.8 g) along with 12 mmol of oleyl alcohol (3.22 g) have been blended with diphenyl ether in order to minimize particles at the nanoscale. (Fig. 2). Finally, the yield for Fe_3O_4-oleate nanoparticles is weighed (2.1 grams).

3.3 Preparation of Nanocomposites

The Fe-OA-PVA nanocomposite films were prepared using 5 g of PVA dissolved in double-distilled water (100ml)and stirred continuously for ~24 h at 40 °C using a magnetic stirrer until the clear solution of PVA. The synthesized Fe_3O_4-oleate was doped at various concentrations (0.25, 0.5, 0.75, and 2wt. %) mixed at 350 rpm for two hours to ensure uniform dispersion. The Fe_3O_4-oleate nanoparticles are disseminated evenly in the polymer solution by stirring the mixture at room temperature. The nanocomposite product was sonicated (Model: USB 1.5L 50, Make: PCI Analytical Pvt. Ltd., Mumbai) at ambient temperature for 15 minutes. The resultant mixture was allowed to relax overnight to eliminate air bubbles. The ensuing viscous solution was poured into immaculate Petri glass plates (S-9, 100 x 15 mm^2) that were placed in a hot air oven (Rotek Instrument) and desiccated at 45 °C for 5 days to remove any residual water. The required amount of Fe_3O_4-oleate was added to the aforementioned clear solution and agitated until the solution became homogenous in order to create the nanocomposite solution. The prepared films were dried to make free from water traces Fig. 3.

The PVA polymer films doped with Fe-OA wt. fractions of 0.25, 0.5, 0.75, 1 and 2 wt. % respectively are prepared using the relation **(1)** [23, 24].

$$M(wt\%) = \frac{m_d}{m_p + m_d} \times 100 \quad \ldots (1)$$

Where m_d is the weight of the dopant and m_p is the weight of the polymer, respectively.

With consideration for any mechanical deformations, the desiccated films have been peeled off carefully. Desiccators were used to preserve these films in order to keep them dry and impurity-free while preventing moisture absorption. The thickness of the film ranging (40 ±2 μm) was tested with a

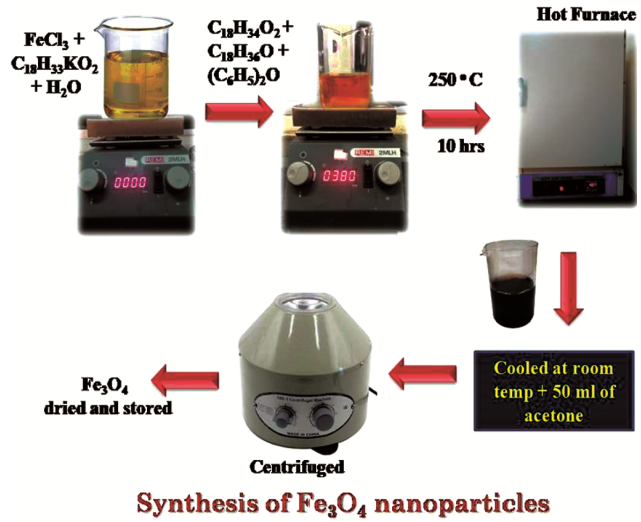

Fig. 2 — Synthesis process of Fe_3O_4 nanoparticles.

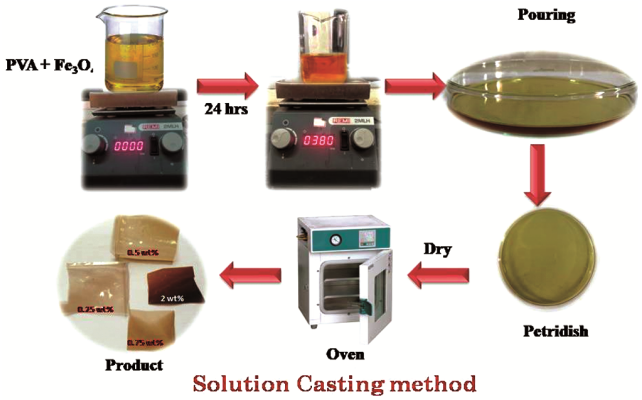

Fig. 3 — Process of solution casting method.

peacock dial thickness gauge (Model: G-2.4N, Ozaki MFG. Co. Ltd.; Japan).

4 Characterization Techniques

The structural, surface morphology, optical, and dielectric properties of Fe-OA-PVA nanocomposite films were studied using different characterization techniques. The identification of functional groups and ion-ion interaction of NPs and PVA was analyzed by FTIR spectroscopy Model PIKE Technologies, Spectrum Two, USA and spectra were recorded in the range of wave number 4000-400 cm^{-1}. UV-Vis (Ultraviolet-visible) spectral data with absorbance mode were captured using a spectrophotometer (DU-730; Beckman Coulter; USA) in the wavelength (λ) range of 200 - 800 nm. X-ray scattering tool Miniflex-II smart lab 3kw; M/s Rigaku, Japan applies Cu-K (λ= 1.5Å) radiation with 2θ angles varying from 10° to 80°, scanning at a rate of 3° min^{-1}, and a minimum step width of 0.02° to get the XRD profiles for Fe-OA-PVA polymer nanocomposites films. The polymer sample of Fe-OA-PVA was placed on a carbon-coated tape for better conductivity. Further, the surface morphological imaging was recorded using (Model; S-3400N, Make; Hitachi, Japan). The EDS spectra were acquired using (Model; Noran System 7, Make; Thermo Fisher Scientific, USA) for identifying elemental composition. Impedance Analyzer (Model; 6500 B, make; Wayne Kerr) were used to record impedance spectroscopy measurements (C_P, D, Z, θ Parameters) at room temperature (27 °C) from 10Hz to 10 kHz at 1 V (ac potential) in SS/Sample/SS (SS; stainless steel) cell combination. The sessile drop approach was used to determine the contact angle of water. The digital camera microscope U-Vision MV500 from China was used to take pictures of the drops.

5 Results and Discussion

The surface morphology of polymer nanocomposites may be regulated by homogeneous dispersion of NPs in a matrix of polymers[23,24]. The effect of oleate as a modulator for tuning the structural, optical, and electrical properties of the polymer matrix has been studied. The Fe NPs interact with the hydrophilic head of the oleate, leaving behind the hydrophobic layer, hence preventing the aggregation of them[25].

5.1 FTIR analysis

The FTIR spectra in transmittance mode reveal the identification of variation in the functional groups and complex formation in unaltered PVA with Fe-OA NPs. The spectra of virgin PVA and its nanocomposite films were measured in the 4000-400 cm^{-1} region, and the data is plotted and obtained as shown in Fig. 4.

IR spectroscopy is an essential technique for detecting functional groups and their chemical properties in polymeric materials. According to Fig. 4, Unaltered PVA has a wide characteristic band that may be seen at roughly 3280 cm^{-1}, 3294 cm^{-1}, and 3296 cm^{-1}. This band is ascribed to –OH stretching vibrations in the PVA matrix. The most characteristic feature of the broadband is observed at OH stretching in Fe-OA-PVAPNPs due to inter and intra-molecular hydrogen bonding. The band shows the polymeric OH stretching for the flexibility of the films. Asymmetric Methyl C-H stretching shows at 2950 cm^{-1} attributed to the saturated aliphatic group. The band at 1727 cm^{-1} moved towards 1721 cm^{-1} is assigned to C=O stretching. The multiple bands between 1447 cm^{-1} and 1290 cm^{-1}, which correspond to CH_2 bending. The band at 1248 cm^{-1} corresponds to C-O-C stretching and the band at 1090 cm^{-1} attributes to –OH stretching. This is due to

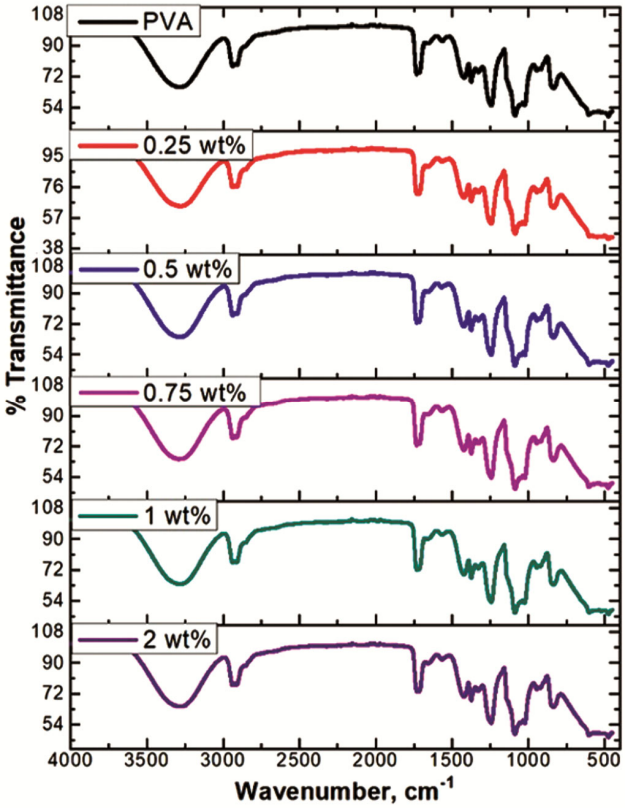

Fig. 4 — FTIR spectra of unaltered PVA and Fe-OA-PVA polymer nanocomposites.

the presence of hydrophobic Fe_3O_4-OA nanoparticles in the film, which increases the hydrophobicity of the film[26,27]. A new band at 470 cm^{-1} corresponds to the Fe-O band in the composite films; this confirms the formation of Fe_3O_4-OA-PVA nanocomposites, and the intensity of this band increased marginally as the Fe_3O_4-OA NPs concentration increased[10]. This substantiates the formation of hydrogen bonds within the PVA matrix. On the basis of these traces of evidence, it can be concluded that Fe_3O_4-OA NPs increase the rigidity of the unaltered PVA film due to the formation of hydrogen bonds and the interaction of OH groups with the Fe_3O_4-OA NPs, which would play a significant role in improving the electrical property of the resulting films[19,25,28,29].

5.2 Optical Analysis

Ultraviolet-Visible spectroscopy is one of the simplest and most efficient optical techniques for investigating the optical and electronic band structure of nanocomposites. The absorption spectra of virgin PVA and Fe_3O_4-OA-PVA nanocomposites films as shown in Fig.5. The absorption spectra of unaltered PVA increase due to increasing the content of Fe_3O_4-OA NPs. The virgin PVA does not display any absorbance peak, which is in agreement with the optical absorption data reported in earlier[30,31]. The absorption peaks observed for all dopant concentration nanocomposites at 223 nm and 325 nm correspond to $\pi \rightarrow \pi^*$ electronic transitions of oleic acid attached to Fe-OA NPs, and it also depends on the polymer chain length and the polymer stereo regularity. Further, the broad peak observed in the visible region occurred at 410 nm due to $\pi \rightarrow \pi^*$ electronic transition for prepared polymer nanocomposites due to the addition of NPs. This attributes an occurrence of Surface Plasmon Resonance (SPR) of Fe-OA NPs in the resulting nanocomposites films as well as charge-transfer (CT) transitions, most likely ligand-metal transitions, to the interaction and complex formations between the dopant and PVA matrix. As the content of Fe-OA NPs in the PVA matrix increased, the spectrum of absorption also shifted to higher wavelengths[32].

5.3 XRD Analysis

The X-ray diffraction study has shown to be a valuable analytical technique for understanding the nanocomposites' underlying microstructure. In the present investigation, XRD was used in order to

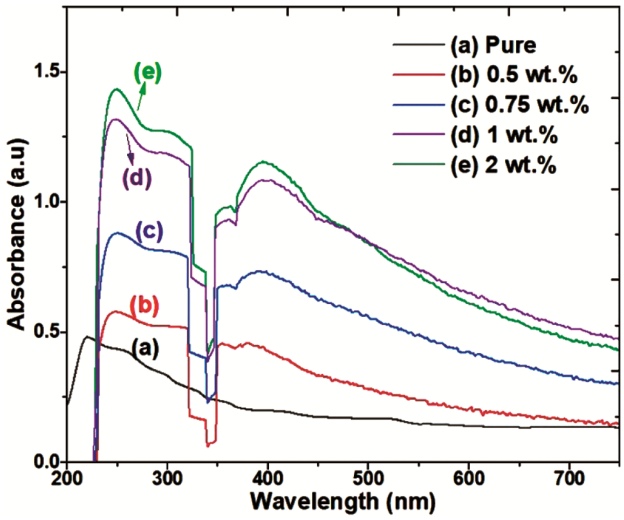

Fig. 5 — UV-Visible absorption spectra of unaltered PVA and different wt. % of Fe-OA- PVA polymer nanocomposites.

investigate the influence of Fe-OA NPs on the morphological modification of the structural and crystalline structure of the PVA polymer matrix. XRD patterns of Oleic acid, Fe_3O_4, unaltered PVA, Fe-OA-PVA polymer nanocomposites at 1 wt. % are presented in Fig.6. The XRD peaks of the NPs and their relative intensity values correspond with known magnetite (Fe_3O_4). Presence of major peaks at/around 11.71°,13.08°, and 14.69° which belongs to oleic acid. The Fe_3O_4 phase was identified by well-defined peaks at/around 20.02°, 46.93°,57.03° and 62.42°, which corresponds to the (1 1 1), (4 0 0), (5 1 1) and (4 4 0) crystallographic diffraction planes as presented in Fig. 6[33]. With a clear appearance in the XRD profile, another sharp peak located at 16.98° which will signify the presence of the crystalline nature of synthesized Fe-OA NPs. Using Scherrer's equation[34,35], the mean crystallite size of Fe-OA NPs obtained below 10 nm. The XRD patterns of PVA exhibit a characteristic peak at around 2θ =19.5°, which indicates that the PVA contains semi-crystalline nature. With the addition of Fe-OA NPs, the PVA matrix's overall XRD profile undergoes several substantial alterations. Based on the XRD profile of the Fe-OA NPs, there are at least eight major peaks at the 2θ values ranging from 10.20° to 65.54°. From Fig. 6, Fe-OA NPs were added, and it was observed that the primary peak in the XRD profile reduced from 19.5° to 19.1°. A strong peak can be seen in the XRD profile of the composite films occurring at 2θ=19.5°, which agrees to a d-spacing value of 4.56Å. This value corresponds to the (101)

plane, which characterizes PVA's semi-crystalline structure. With an increase in Fe-OA NPs, this characteristic peak's intensity was proportionally reduced. This occurs due to the development of hydrogen bonds and interactions between –OH groups and Fe-OA NPs[36,37]. This impact is particularly prominent due to the fact that the amount of Fe-OA NPs efficiently increased in the films.

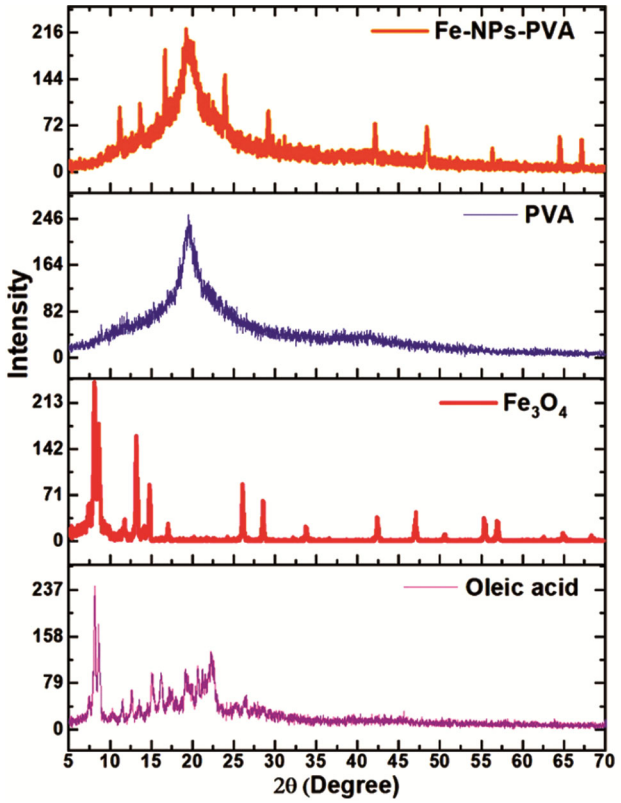

Fig. 6 — XRD profiles of a) oleic acid, b) Fe_3O_4, c) Unaltered PVA, d) Fe-OA-PVA polymer nanocomposites at 1 wt.%.

5.4 SEM Analysis

The scanning electron microscope (SEM) was used to investigate the morphology and the degree of dispersion that exists, as well as the compatibility of Fe_3O_4-OA NPs that were doped with PVA. Fig. 7 illustrates the SEM images of the surface morphology of unaltered PVA and Fe-OA-PVA polymer nanocomposites with doping percentages of 0.25, 0.5, 0.75, 1 and 2 wt.%. All samples were prepared as per the protocol with gold sputtering, and images were acquired in the condition of Vac 5 kV with a scale of 20 µm. Fe_3O_4-OA NPs were equally dispersed throughout the PVA matrix, as shown in SEM images. As we increase the doping concentration of Fe_3O_4-OA NPs without any break in the polymer, the NPs are well distributed in PVA. The same is observed in different images in Fig 7. Images clearly demonstrate that Fe_3O_4-OA NPs inserted into the polymer matrix do not have any voids around them. This assures that Fe_3O_4-OA NPs were added to polymer films and that those films are devoid of any potential flaws. Consequently, it is not difficult to use the generated nanocomposite polymers for electrical processes [38].

5.5 EDS Analysis

Element inspection of the produced Fe_3O_4-OA-PVA nanocomposites was performed using energy-dispersive X-ray spectroscopy.EDS is used to examine the polymer film's composition and observe the incorporation of well-sulfonated Fe_3O_4 NPs. In Fig. 8, we observed that initially, in unaltered PVA spectra, only 'C' and 'O' elements were present with wt. % of 52.92 and 46.93, respectively. In Fe_3O_4– OA spectra, we observed the strong 'O' peak with wt. % of

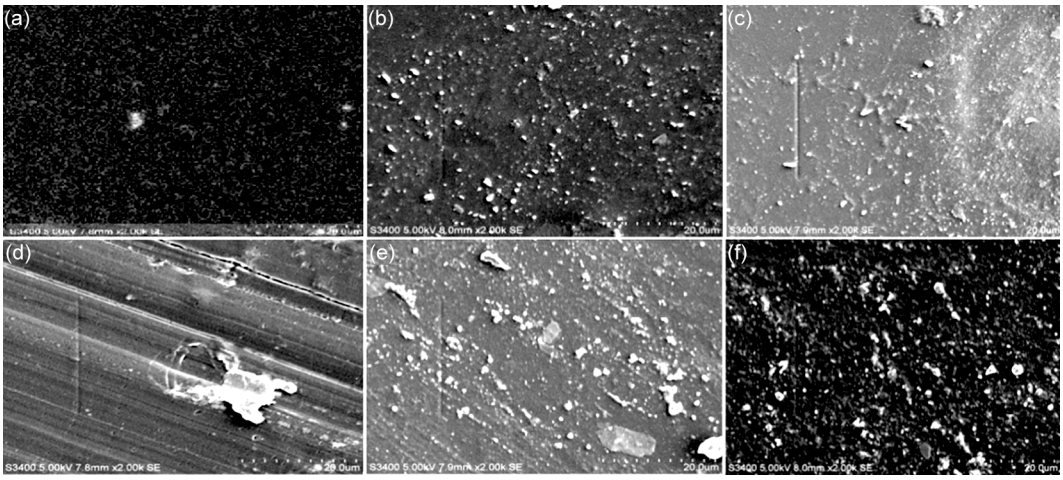

Fig. 7 — SEM images of a) Unaltered PVA, b) 0.25, c) 0.5, d) 0.75, e) 1 and f) 2 wt. % of Fe-OA-PVA nanocomposites.

32.86 and 67.14 of 'Fe'. As we dope Fe_3O_4– OA to polymer, the 'C', 'O', and 'Fe' are dominantly present. In 1 wt. % of Fe_3O_4-OA-PVA nanocomposites, we observed 48.94%, 43.98%, and 4.83% of 'C', 'O' and 'Fe' respectively. Similarly, in 2 wt. % spectra we observed 'C' with 54.04%, 'O' with 40.90%, and 'Fe' with 5.06%. For the lower concentration of Fe_3O_4-OA (0.25%, 0.5% and 0.75%), we did not observe any remarkable peak of Fe. But as we increase the wt. % from 1wt. % to 2wt. % we successfully observed Fe peak. So, in Fig. 8, we showed the spectra of unaltered PVA, Fe_3O_4-OA, 1 wt. % and 2 wt. % only.

5.6 Contact Angle Measurement

One of the most well-known techniques for examining the surface characteristics of films is contact angle measurement. In order to directly assess surface wettability, this research employed geometric measures or angles created at the junction of the liquid, gas, or solid phases[23]. Contact angle values of water were measured for all prepared Fe-OA-PVA polymer nanocomposite films at 1 µl at room temperature. The fluctuation in contact angle with varied quantities of Fe-OA NPs concentration in the PVA matrix is shown in Fig. 9. The Fe-OA-PVA polymer nanocomposites' determined surface energy and contact angle values are tabulated in Table.1.

The hydrophilic character of the nanocomposite films switches to a hydrophobic nature, as shown by the contact angle of the polymer nanocomposite films, which ranges between 72.6° to 87.0°. It might be explained by the fact that increasing more NPs to films causes more hydrogen bonds to form between the Fe-OA particles, the PVA -OH group, and the polar groups in the PVA bud's fluid, which reduces the likelihood that an incoming water molecule would connect with the particles[39]. Employing the Owens-Wendt formula[40], the wettability aspects of the prepared polymer nanocomposite films were observed to estimate total Surface Free Energies (SFE). The estimated surface free energy values ranged between 92.7 and 74.6 mJ/, respectively. According to these findings, the incorporation of Fe-OA NPs into polymer nanocomposites leads to an increase in hydrophobicity while simultaneously leading to a reduction in surface energy[23]. This may be due to the hydrophobic nature of the Fe-OA NPs filler[41].

5.7 Dielectric Properties

The constant increase in the demand for the preparation of novel microelectronic devices with enhanced functionality, performance and water-repellent miniatures resulted in the development of polymer nanocomposites consisting of conducting fillers. The addition of fillers will bring various advantages, including high thermal stability and

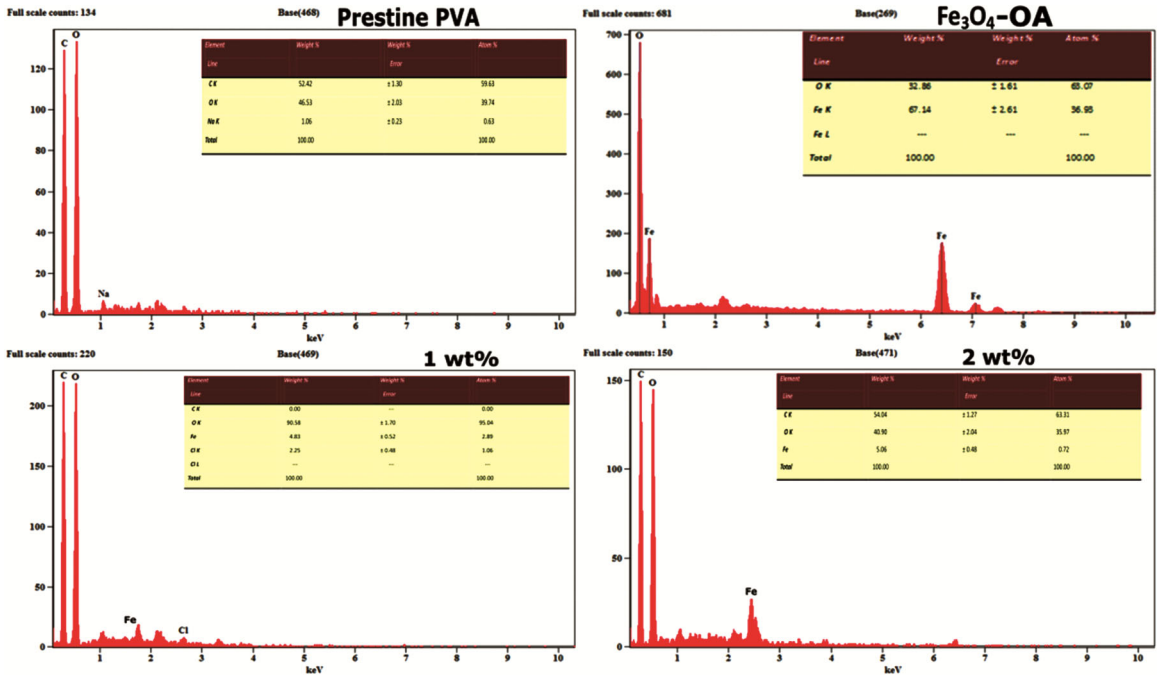

Fig. 8 — Energy dispersive spectroscopic analysis (EDS) of Fe_3O_4-OA-PVA nanocomposites.

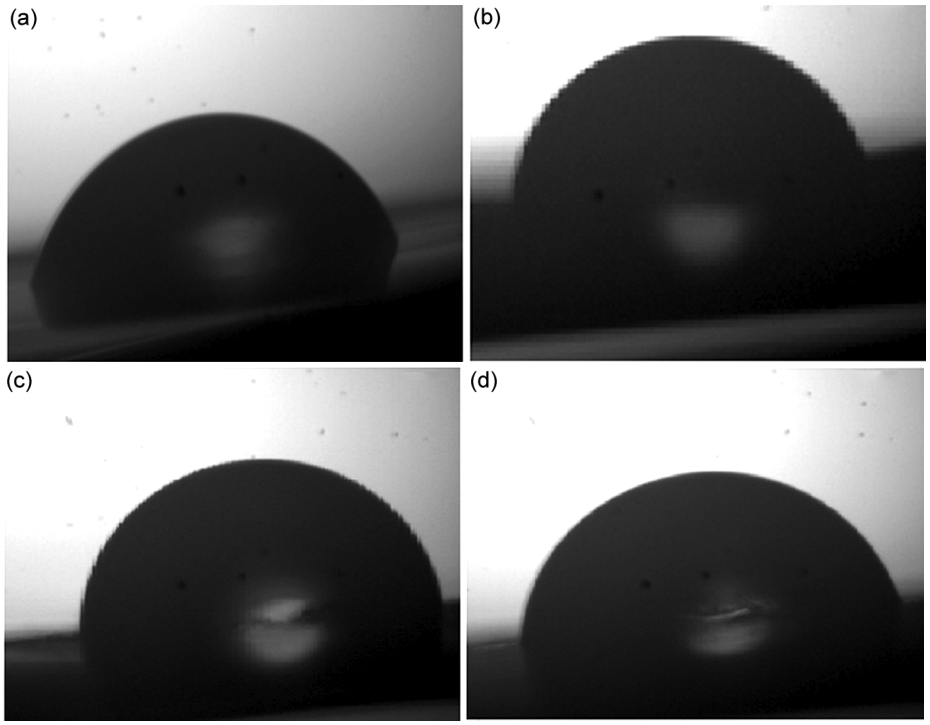

Fig. 9 — Images of water droplets on the surface, including their contact angles and shapes of (a) Unaltered PVA (b) 0.5wt. % (c) 1 wt. % and (d) 2 wt. % of Fe-OA NPs in polymer nanocomposite thin films.

Table 1 — Contact angle and surface energy of the Fe-OA-PVA nanocomposites system.

Fe-OA NPs in PVA (Wt. %)	Contact angle (degree)	Surface energy (mJ/m^2)
Unaltered PVA	72.6	92.7
0.5wt. %	77.9	88.8
1wt. %	80.3	86.1
2wt. %	87.0	74.6

improved flexibility. The materials must have a large dielectric constant and a small dielectric loss for capacitor applications. One such material in this regard is the organic-inorganic hybrid nanocomposites embedded in the polymer matrix; these materials show an enhanced dielectric constant[11,12,23]. In this investigation, an effort was made to design and develop Fe_3O_4-OA-PVA composites with a high dielectric constant and a low dielectric loss.

To quantify the storage of electrical energy in the materials, the dielectric properties of nanocomposite films have been investigated. The dielectric feature of a material is found to depend on its permittivity and capacitance(C_p), as well as the shape and 3D array (arrangement) of the nano fillers[23,42,43]. The relative function of permittivity and dielectric loss of nanocomposites is given by equation (2)[16].

$$\varepsilon''(\omega) = \varepsilon' - i\varepsilon'' \quad \ldots (2)$$

Where ε′ is the dielectric constant and $i\varepsilon''$ is the imaginary part permittivity and are illustrative components of storage and loss.

5.8 Dielectric Constant

The dielectric constant, which may be influenced by a number of factors, including temperature, the frequency of the electric field, the thickness of the material, humidity, the effects of radiation, mechanical stress, *etc*., is the total electric charge which can be stored in a capacitor. The dielectric constant (ε′) of Fe_3O_4-oleate-PVA nanocomposites has been inferred from the capacitance values[16].

$$\varepsilon' = \frac{Ct}{\varepsilon_o A} \quad \ldots (3)$$

Where C is the capacitance, and it depends on electrode area along with properties of the dielectric (insulator) material used, t is the thickness of the polymer nanocomposite film or dielectric layer, ε_o= permittivity of free space, and A is the area of the stainless-steel electrode.

Filler content has a beneficial impact on the dielectric constant (ε′), as illustrated by a plot of dielectric constant v/s nanoparticle concentration. From Fig. 10, the ε′ (dielectric constant) shows a maximum of 2 wt. % of Fe-OA/PVA nanocomposites is attributed to the contribution of Maxwell-Wegner ionic conduction and the increase of Fe-OA NPs content[44]. This emphasizes the application of thin film as the dielectric layer for charge storage applications. Due to the orientation of electrical charges and field-induced parting, thin films are capable of storing electrical charges. Also, a mini capacitor network formation in the thin films with the increase in the filler content was shown in Fig. 10. It demonstrates a decrease in the dielectric property as frequency increases; in simpler terms, A material's dielectric constant increases in a linear fashion with enhancing particle size[44]. Furthermore, the longer relaxation time suggested by, the higher dielectric constant values perceived at lower frequencies aids in the successful alignment of the dipoles, making increased polarization. In particular, the material's net polarization diminishes with increasing frequency because each polarization mechanism contributes less and less, and the dielectric constant drastically drops as a result. However, a persistent decrease in space charge and a lower dielectric constant at higher frequencies is referred to as a result of the slow movement of the charge carriers hindered or confined inside the polymer matrix. These results are matches with some other polymer nanocomposite systems[22].

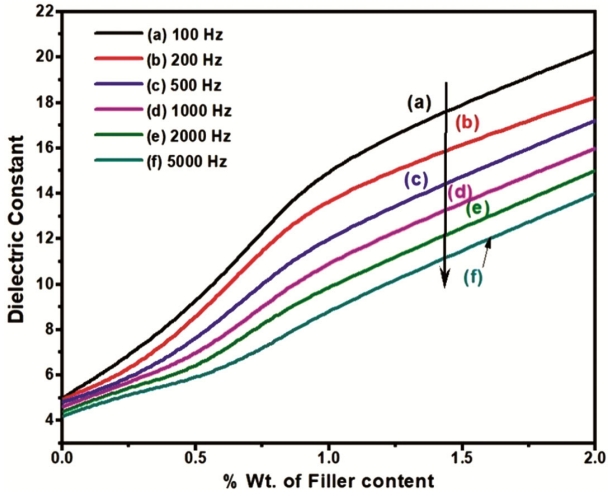

Fig. 10 — Difference of dielectric constant of Fe-OA-PVA nano composites of 0.25, 0.5, 0.75, 1, and 2 wt. % of Fe-OA NPs at different frequency range.

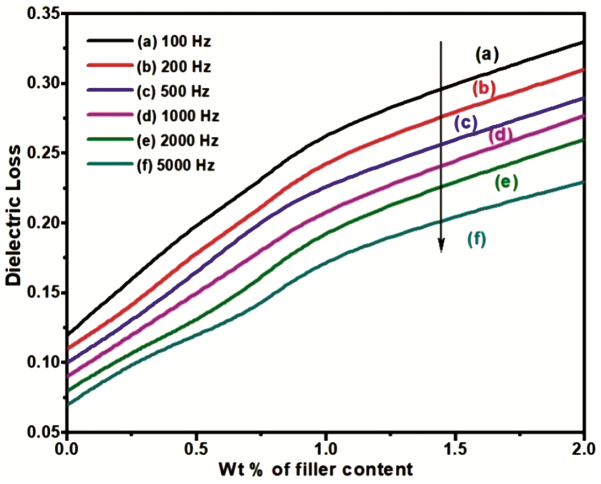

Fig. 11 — Difference of Dielectric Loss of Fe-OA-PVA nanocomposite system of 0.25, 0.5, 0.75, 1 and 2 wt % of Fe-OA NPs at different frequency range.

5.9 Dielectric Loss

Three main mechanisms, including DC (Direct Current) conduction, Space Charge Migration (interfacial polarization contribution), and movement of the molecular dipoles (dipole losses), are often responsible for the dielectric loss of dielectric materials. The dielectric loss is due to the loss of energy due to the microscopic Brownian motion of electric dipoles, resulting in a loss that depends on the viscosity of the system[44]. A dielectric material's intrinsic capacity to dissipate electromagnetic energy is measured by its dielectric loss (ε ″)[16,38]. The dielectric loss is also known as the loss factor; the dissipative of a material is measured due to an external field. The correlation between dielectric loss and NPs (filler) content at various frequencies is seen in Fig. 11. The graph shows that the dielectric loss rises with the amount of filler present and is caused by charge polarization that is produced by the polarization that is brought on by the presence of nanoparticles. Additionally, a sharp reduction in the dielectric loss is shown as frequency increases. The polarization processes, such as orientation, space charge distribution, and ions, start to lag following the applied field as its frequency increases, which reduces dielectric loss[44]. It is possible that the mobilization of charges inside the polymer matrix is to blame for the greater dielectric loss that occurs at a frequency that is substantially lower. At a higher frequency, however, there is a reversal of the field, resulting in a decrease in charge aggregation and dielectric loss.

5.10 Loss Tangent

The loss tangent value can be obtained by knowing the values of dielectric constant(ε') and dielectric loss (ε'') and is calculated by following the relation[44].

$$\varepsilon'' = \varepsilon' \tan(\delta) \quad \ldots (4)$$

Where δ is the phase angle between the dielectric polarization and dielectric field.

The variation of loss tangent against filler concentration at varying frequencies is shown in Fig. 12. The graph shows an increase in loss tangent with an increase in filler content. The increase in filler content resulted in a decrease in the inter-particle distance, consequently resulting in decreased charge trapping sites. In the first region (0.25 wt. % to 0.75 wt. %) with fixed lower frequency (100, 2000 Hz), the dielectric loss tangent graph displayed a small peak for 0.25 wt. % of prepared Fe-OA nanocomposites. That may be due to the semi-crystalline nature of the composite material, and the orderliness gets raised with the addition of dopant nanoparticles. In the second region (0.75 wt. % to 2wt. %) same small peak raised in 1wt % for all lower and higher fixed frequencies. This is maybe due to initiated dipolar polarization of the polymer chains in the pure blend and/or dipolar polarization of the polymer chain, as well as filler molecules in the composites[45,46].

5.11 AC Conductivity

Understanding the nature of the charge transfer mechanism, the electrical conductivity of Fe-OA-PVA nanocomposite films has been investigated in a heterogeneous system. AC conductivity (σ_{ac}) is a feature of a material that changes with frequency. It is caused by the fluctuating motion of charge carriers in the polymer system. The AC conductivity was measured using the values of obtained conductance[17].

$$\sigma_{ac} = d\frac{G_s}{A} \quad \ldots (5)$$

Where d is the thickness of the nanocomposite film, A is the area of the SS electrode, and G_s is the conductance value.

The filler content shows the change in conductivity. They illustrate that dopants are the reason for the polarization of electrons. The Fe_3O_4-OA contributes to the accumulation of charges and leads to the formation of dipoles on PVA clusters. In Fig. 13, we can observe that the AC conductivity

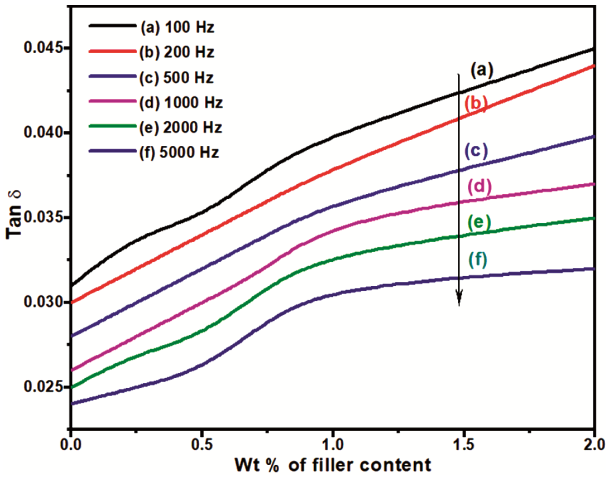

Fig. 12 — Difference of loss tangent($\tan \emptyset$) of Fe-OA-PVA nanocomposites films of 0.25, 0.5, 0.75, 1 and 2 wt.% of Fe-OA NPs at various frequency range.

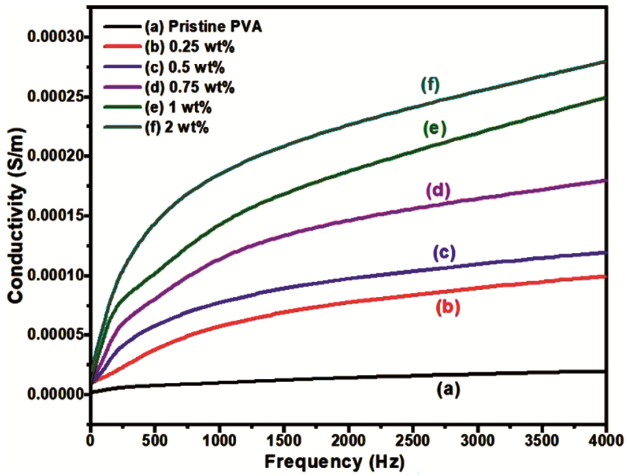

Fig. 13 — AC conductivity of Fe-OA-PVA nanocomposite films of 0.25, 0.5, 0.75, 1 and 2 wt% of Fe-OA NPs with varying frequency.

increased with the frequency for an increase in wt. % of dopant. This is because of the localized charge carrier. So, due to dopant concentration, the charge carrier concentration increased and for a higher frequency, the mobility increased within the PVA[47]. The inclusion of filler material fills up the fault areas in the polymer matrix, decreasing the potential barrier for charge transfer. At higher frequencies, electrons have enough energy to jump from one location to another through a hopeful process, resulting in greater electrical conductance with frequency.

6 Conclusions

In this investigation, Fe_3O_4 nanoparticles were synthesized by the chemical reduction method. The

powdered nanoparticles are modified with oleic acid. The obtained Fe-OA NPs have been incorporated in a poly (vinyl alcohol) matrix with different wt. % using solvent casting technique. FTIR analyses of polymer nanocomposites revealed the existence of iron oxide nanoparticles (Fe-OA NPs) and their interaction with polyvinyl alcohol (PVA) across H-bonding. This interaction is further validated by the fact that the strength of the peak shifts, as well as the fact that band broadening occurs in the powder XRD spectra. The UV-visible investigation reveals that there is a presence of a variety of electronic transitions inside the nanocomposites, as well as an increase in absorbance with increasing filler content. The SEM images of nanocomposite films show the circular shape of Fe-OA NPs. Also, we observed the increase in roughness with an increase in filler content due to filler and PVA interaction and excellent distribution of Fe-OA NPs into PVA. From contact angle measurements, the addition of Fe-OA NPs boosted the hydrophobicity and decreased the surface energy of prepared Fe-OA polymer nanocomposites. According to dielectric properties, the dielectric constant and dielectric loss of the prepared polymer nanocomposite films increased with increasing filler concentration but decreased with increasing frequency. Additionally, the increase in filler content and frequency led to an increase in the AC conductivity of the prepared films. These results suggested that the prepared polymer nanocomposites are adaptable to energy storage applications without loss of flexibility, stability, and scalability.

Acknowledgement

The authors are thankful to USIC & SAIF, Karnatak University, Dharwad for providing experimental facilities and DST/SERB, Govt. of India, for sanctioning the research project (SB/EMEQ-089/2013). With respect and admiration for providing UGC-JRF/SRF support (518772/Dec 2015), Author Chetan Chavan thanks to University Grants Commission (UGC), New Delhi. The authors are thankful to UGC, New Delhi, for providing research grants under SAP-CAS Phase-II (F.530/9/CAS-II/2015 (SAP-I). Author Kanakaraj T. M. is thankful to J S S Arts, Science and Commerce College, Gokak, for valuable support.

References

1 Khan I, Saeed K & Khan I, *Arab J Chem*, 12 (2019) 908.
2 Bulla S S, Chavan C & Bhajantri R F, *J Inorg Organomet Polym Mater*, 31 (2021) 2368.
3 Arias LS, Pessan J P, Vieira A P M, Lima T M T d, Delbem A C B & Monteiro D R, *Antibiotics*,7 (2018) 46.
4 Camargo P H C, Satyanarayana K G & Wypych F, *Mater Res*, 12 (2009) 1.
5 Gulotty R, Castellino M, Jagdale P, Tagliaferro A & Balandin A A, *ACS Nano*, 7 (2013) 5114.
6 Laxmeshwar S S, Viveka S, Madhu Kumar D J, Dinesha, Bhajanthri R F & Nagaraja G K, *J Macromol Sci Part A Pure Appl Chem*, 49 (2012) 639.
7 Gaaz T S, Sulong A B, Akhtar M N, Kadhum A A H, Mohamad A B & Al-Amiery A A, *Molecules*, 20 (2015) 22833.
8 Kamoun E A, Chen X, Mohy Eldin M S & Kenawy E R S, *Arab J Chem*, 8 (2015) 1.
9 Anandalli M H, Bhajantri R F, Maidur S R & Patil P S, *J Mater Sci Mater Electron*, 31 (2020) 10531.
10 Hoque M A, Ahmed M R, Rahman G T, Rahman M T, Islam M A, Mubarak A Khan & Khalid Hossain M, *Results Phys*, 10 (2018) 434.
11 Hanemann T & Szabó D V, *Materials (Basel)*, 3 (2010) 3468.
12 Fu S, Sun Z, Huang P, Li Y & Hu N, *Nano Mater Sci*, 1 (2019) 2.
13 Bernal-Ballen, Lopez-Garcia J-A & Ozaltin K, *Polymers (Basel)*, 1325 (2019) 1.
14 Homaei A A, Sariri R, Vianello F & Stevanato R, *J Chem Biol*, 6 (2013) 185.
15 Luzi F, Torre L, Kenny J M & Puglia D, *Materials*, 12 (2019) 471.
16 Hebbar V, Bhajantri R F & Naik J, *J Mater Sci Mater Electron*, 28 (2017) 5827.
17 Bhajantri R F, Ravindrachary V, Harisha A, Crasta V, Nayak S P & Poojary B, *Polymer (Guildf)*, 47 (2006) 3591.
18 Rithin K N B, Crasta V, Bhajantri R F & Praveen B M, *J Polym*, 2014 (2014) 1.
19 Chandrakala H N, Ramaraj B, Shivakumaraiah, Lee J H & Siddaramaiah, *J Alloys Compd*, 580 (2013) 392.
20 Bhattacharya M, *Materials (Basel)*, 9 (2016) 262.
21 Sheela T, Bhajantri R F & Ravindrachary V, *AIP Conf Proc*, 1512 (2013) 1302.
22 Ravindrachary V, Bhajantri R F, Harisha A, Ismayil C & Ranganathaiah, *Phys Status Solidi Curr Top Solid State Phys*, 6 (2009) 2438.
23 Subramani N K, Kasargod Nagaraj S, Shivanna S & Siddaramaiah H, *Macromolecules*, 49 (2016) 2791.
24 Thimmaiah S, Bhajantri R F, Nambissan P M G, Vasachar R, Rathod S G & P Boja, *J Appl Polym Sci*, 132 (2015) 1.
25 Bhajantri R F, Ravindrachary V, Harisha A, Ranganathaiah C & Kumaraswamy G N, *Appl Phys A Mater Sci Process*, 87 (2007) 797.
26 Pujar M S, Hunagund S M, Barretto D A, Desai V R, Patil S, Vootla S K & Sidarai A H, *Bull Mater Sci*, 43 (2019) 24.
27 Coates J, *Encycl Anal Chem*, (2006).
28 Hammannavar P B, Baraker B M, Bhajantri R F, Ravindrachary V & Lobo B, *J Phys Conf Ser*, 618 (2015).

29 Ismayil, Vasachar R, Bhajantri R F, Dhola P S & Sanjeev G, *Nucl Instruments Methods Phys Res Sect B: Beam Interact with Mater Atoms*, 342 (2015) 29.
30 Bhajantri R F, Ravindrachary V, Harisha A, Ismayil C & Ranganathaiah, *Phys Status Solidi Curr Top Solid State Phys*, 6 (2009) 2429.
31 Khanna P K, Gokhale R R, Subbarao V V, Singh N, Jun K W & Das B K, et al., *Mater Chem Phys*, 94 (2005) 454.
32 Amin G A M & Abd-El Salam M H, *Mater Res Express*, 1 (2014) 25024.
33 Wang D, Ma Q & Yang P, *J Nanosci Nanotechnol*, 12 (2012) 6432.
34 Chouhan S, Bhatt R, Bajpai A K, Bajpai J & Katare R, *Fibers Polym*, 16 (2015) 1243.
35 Pujar M S, Hunagund S M, Desai V R, Patil S & Sidarai A H, *AIP Conf Proc*, 1942 (2018) 050026.
36 Kim S Y, Ramaraj B & Yoon K R, *Surf Interface Anal*, 44 (2012) 1238.
37 Riva I I, Wulandari I O, Sulistyarti H & Sabarudin A, *IOP Conf Ser Mater Sci Eng*, 299 (2018) 012065.
38 El Sayed A M & Morsi W M, *J Mater Sci*, 49 (2014) 5378.
39 Goudar N, Vanjeri V N, Kasai D, Kasai D, Gouripur G, Malabadi R B, Masti S P & Chougale R B, *J Polym Environ*, 29 (2021) 2797.
40 Firlik Sebastian & Molenda Jaroslaw B J, *Chemik*, 64 (2010) 242.
41 Kim J H, Shin D S, Han M H, Kwon O W, Lee H K, Lee S G, Ghim H D, Park J M, Han S S, Noh S K & Lyoo W S, *J Appl Polym Sci*, 105 (2007) 424.
42 Chandrakala H N, Ramaraj B, Shivakumaraiah, Madhu G M & Siddaramaiah, *J Mater Sci*, 47 (2012) 8076.
43 Wang D, Bao Y, Zha J W, Zhao J, Dang Z M & Hu G H, *ACS Appl Mater Interfaces*, 4 (2012) 6273.
44 Rayssi C, El Kossi S, Dhahri J & Khirouni K, *RSC Adv*, 8 (2018) 17139.
45 Sengwa R J & Dhatarwal P, *Electrochim Acta*, 338 (2020) 135890.
46 Dhatarwal P, Choudhary S & Sengwa R J, *Polym Bull*, 78 (2021) 2357.
47 Minea A A, *Nanomaterials*, 9 (2019) 1592 .